

Future sea-level rise from tidewater and ice-shelf tributary glaciers of the Antarctic Peninsula

Schannwell, Clemens; Barrand, Nicholas; Radic, Valentina

DOI:

[10.1016/j.epsl.2016.07.054](https://doi.org/10.1016/j.epsl.2016.07.054)

License:

Creative Commons: Attribution-NonCommercial-NoDerivs (CC BY-NC-ND)

Document Version

Peer reviewed version

Citation for published version (Harvard):

Schannwell, C, Barrand, N & Radic, V 2016, 'Future sea-level rise from tidewater and ice-shelf tributary glaciers of the Antarctic Peninsula', *Earth and Planetary Science Letters*, vol. 453, pp. 161–170.

<https://doi.org/10.1016/j.epsl.2016.07.054>

[Link to publication on Research at Birmingham portal](#)

Publisher Rights Statement:

Checked for eligibility: 12/08/2016

General rights

Unless a licence is specified above, all rights (including copyright and moral rights) in this document are retained by the authors and/or the copyright holders. The express permission of the copyright holder must be obtained for any use of this material other than for purposes permitted by law.

- Users may freely distribute the URL that is used to identify this publication.
- Users may download and/or print one copy of the publication from the University of Birmingham research portal for the purpose of private study or non-commercial research.
- User may use extracts from the document in line with the concept of 'fair dealing' under the Copyright, Designs and Patents Act 1988 (?)
- Users may not further distribute the material nor use it for the purposes of commercial gain.

Where a licence is displayed above, please note the terms and conditions of the licence govern your use of this document.

When citing, please reference the published version.

Take down policy

While the University of Birmingham exercises care and attention in making items available there are rare occasions when an item has been uploaded in error or has been deemed to be commercially or otherwise sensitive.

If you believe that this is the case for this document, please contact UBIRA@lists.bham.ac.uk providing details and we will remove access to the work immediately and investigate.

Future sea-level rise from tidewater glaciers and ice-shelf tributary glaciers of the Antarctic Peninsula

Clemens Schannwell^{a,b}, Nicholas E. Barrand^a, Valentina Radić^c

^a*School of Geography, Earth and Environmental Sciences, University of Birmingham, Birmingham, UK*

^b*British Antarctic Survey, Natural Environment Research Council, Cambridge, UK*

^c*Department of Earth, Ocean and Atmospheric Sciences, University of British Columbia, Vancouver, British Columbia, Canada*

Abstract

Iceberg calving and increased ice discharge from ice-shelf tributary glaciers contribute significant amounts to global sea-level rise (SLR) from the Antarctic Peninsula (AP). Owing to ongoing ice dynamical changes (collapse of buttressing ice shelves), these contributions have accelerated in recent years. As the AP is one of the fastest warming regions on Earth, further ice dynamical adjustment (increased ice discharge) is expected over the next two centuries. In this paper, the first regional SLR projection of the AP from both iceberg calving and increased ice discharge from ice-shelf tributary glaciers in response to ice-shelf collapse is presented. An ice-sheet model forced by temperature output from 13 global climate models (GCMs), in response to the high greenhouse gas emission scenario (RCP8.5), projects AP contribution to SLR of 28 ± 16 to 32 ± 16 mm by 2300 that is roughly split between tidewater glaciers and ice-shelf tributary glaciers. In the RCP4.5 scenario, sea-level rise projections to 2300 are dominated by tidewater glaciers (~ 8 -18 mm). In this

Email address: `cxs400@bham.ac.uk` (Clemens Schannwell)

cooler scenario, 2.4 ± 1 mm is added to global sea levels from ice-shelf tributary drainage basins as fewer ice-shelves are projected to collapse. Sea-level projections from ice-shelf tributary glaciers are dominated by drainage basins feeding George VI Ice Shelf, accounting for $\sim 70\%$ of simulated SLR. Combined total ice dynamical SLR projections to 2300 from the AP vary between 11 ± 2 and 32 ± 16 mm sea-level equivalent (SLE), depending on the emission scenario used. These simulations suggest that omission of tidewater glaciers could lead to a substantial underestimation of the ice-sheet's contribution to regional SLR.

Keywords: Ice dynamics, Sea-level rise, Tidewater glaciers, Ice-shelf collapse, Ice-shelf tributary glaciers

1. Introduction

The Antarctic Peninsula (AP) is a mountainous and heavily glaciated region, dominated by glaciers flowing directly into the sea (henceforth tidewater glaciers) and into floating ice-shelves (henceforth ice-shelf tributary glaciers). In response to the rapid warming experienced by this region over the last 50 years (*Vaughan et al.*, 2003), glaciers have contributed at an accelerated rate to global sea-level rise (SLR) in recent years (*Cook et al.*, 2005; *Wouters et al.*, 2015). In addition to an increase in near-surface air temperatures, surface waters of the surrounding ocean have warmed (*Meredith and King*, 2005). This ocean warming has been accompanied by an acceleration (*Pritchard and Vaughan*, 2007) and retreat (*Cook et al.*, 2005) of tidewater glaciers, leading to increased ice discharge to the ocean. Climatological changes have also affected ice-shelf tributary glaciers. Un-

14 like tidewater glaciers, ice-shelf tributary glaciers do not flow directly into
15 the ocean, but into a floating ice-shelf. This extension of the grounded ice
16 exerts backstress (buttressing force) on the grounded glacier upstream and
17 thus restrains ice flow. If this buttressing force is reduced or removed, the
18 grounded ice upstream will speed up, thin and discharge more ice into the
19 ocean. This behaviour has been observed at several locations in the AP re-
20 gion (*Rott et al.*, 2002; *Scambos et al.*, 2004; *Rignot et al.*, 2004). Glaciers
21 draining into the Prince-Gustav-Channel and Larsen A embayments are still
22 adjusting to ice-shelf removal, some 20 years after ice-shelf collapse (*Rott*
23 *et al.*, 2014; *Scambos et al.*, 2014), and are contributing a significant portion
24 to the region’s SLR (*McMillan et al.*, 2014).

25 Abrupt ice-shelf collapse events in the past have been linked to a combi-
26 nation of atmospheric warming (*Vaughan and Doake*, 1996; *Scambos et al.*,
27 2000) and increased basal melting (*Pritchard et al.*, 2012; *Holland et al.*,
28 2015). Ice-shelves are thought to be structurally weakened prior to collapse
29 by i) hydrofracture of surface crevasses, and ii) basal melting at the ice-ocean
30 interface. In the latter process, warm ocean water erodes the underside of
31 the ice-shelf, thinning it and thus leaving the ice-shelf more vulnerable to
32 the process of hydrofracturing (*Shepherd et al.*, 2003). Hydrofracture of sur-
33 face crevasses occurs primarily when sufficient meltwater is available at the
34 surface of the ice-shelf and can wedge open crevasses to cause catastrophic
35 ice-shelf disintegration (*Scambos et al.*, 2004). Recent studies suggest that
36 other ice-shelf weakening processes such as fracturing and weakening of shear
37 margins may also be important and lead to a progressive weakening of the
38 ice-shelf prior to disintegration (*Khazendar et al.*, 2015; *Borstad et al.*, 2016).

39 A prime example of this is the progressive mechanical weakening of remnant
 40 Larsen B Ice Shelf over the last 15 years (*Borstad et al.*, 2016). The impor-
 41 tance of these processes may however vary for individual ice-shelves.
 42 While projections of the surface mass balance are forecasted to provide a
 43 negative contribution to sea level, this is expected to be offset by sea-level
 44 rise contributions from ice dynamical changes (*Barrand et al.*, 2013a). Owing
 45 to their short response times to ice dynamical perturbations, e.g. ice-shelf
 46 removal, in comparison to the rest of the Antarctic Ice Sheet (*Barrand et al.*,
 47 2013a), AP glaciers are projected to play an important role in the global
 48 SLR budget over the next century (*Barrand et al.*, 2013a; *Schannwell et al.*,
 49 2015). Hitherto, ice-sheet modelling studies of the AP have focused on SLR
 50 projections from ice-shelf tributary glaciers, ignoring any contributions from
 51 tidewater glaciers (*Barrand et al.*, 2013a; *Schannwell et al.*, 2015). Given
 52 the observed acceleration and retreat of most tidewater glaciers (*Cook et al.*,
 53 2005; *Pritchard and Vaughan*, 2007), this may lead to a substantial underes-
 54 timation of the SLR contribution from the AP. In this paper, we present the
 55 first comprehensive modelling study of SLR projections from both tidewater
 56 and ice-shelf tributary glaciers of the AP. Building on the work of *Schannwell*
 57 *et al.* (2015), ice-shelf collapse timing is not determined by thermal viability
 58 limits, but is instead based on the total number of melt days - a more direct
 59 and physically-based link to the process of hydrofracture. Daily instead of
 60 monthly near-surface temperature projections are used to estimate timing
 61 of future ice-shelf collapse events. To estimate grounding line retreat in re-
 62 sponse to ice-shelf removal, a new statistical framework is introduced that
 63 builds on previous work by *Schannwell et al.* (2015), but improves upon their

64 statistical parameterisation by relating expected grounding line retreat to the
 65 degree of buttressing. Buttressing for each drainage basin at the grounding
 66 line is calculated by dividing the normal pressure in presence of an ice-shelf
 67 by the ocean pressure acting when no ice-shelf is present. The combined SLR
 68 contribution over the next 300 years is computed, including for the first time
 69 the largest 235 tidewater glaciers throughout the northern AP. In addition
 70 to this, volume responses of the largest 215 ice-shelf tributary glaciers are
 71 simulated. These 450 drainage basins cover a total of 77% of the AP's area,
 72 providing a comprehensive coverage of the Antarctic Peninsula Ice Sheet
 73 (APIS).

74 **2. Data and Methods**

75 *2.1. Climate data and preprocessing*

76 In order to estimate the timing of future ice-shelf collapse events, daily
 77 near-surface temperature fields from 13 GCMs from the Coupled Model In-
 78 tercomparison Project Phase 5 (CMIP5) (*Taylor et al.*, 2011) were selected
 79 using the Representative Concentration Pathway (RCP)4.5 (*Vuuren et al.*,
 80 2011) and RCP8.5 emission scenarios. The selection of the GCM forcings
 81 are provided in Figure A.6 and follows *Schannwell et al.* (2015). Tempera-
 82 ture projection fields were bias-corrected against monthly ERA-Interim data
 83 from the European Centre for Medium Range Weather Forecasts (ECMWF;
 84 *Dee et al.*, 2011) by shifting the future temperature fields by the average
 85 bias for each month between the GCM and ERA-Interim temperatures over
 86 the period 1979-2005 (*Radić et al.*, 2014). The bias-corrected temperatures
 87 were then compared to surface station data (Table B.2) from the AP. The

88 remaining temperature difference between bias-corrected temperature fields
 89 and surface station data is attributed to an inaccurate height representa-
 90 tion in the temperature fields caused by the relative coarse spatial resolution
 91 of the models ($\sim 0.75^\circ$). Owing to the rugged topography of the AP, this
 92 can introduce significant temperature differences (*Jones and Lister, 2014*).
 93 To correct for this, temperature fields were shifted by a temperature-height
 94 correction factor derived for each month from every station. As most sur-
 95 face stations are clustered in the north of the AP, temperature data from
 96 automatic weather stations were additionally included to improve spatial
 97 coverage. A list of stations is provided in the appendix (Table B.2). Height
 98 correction factors were then bi-linearly interpolated and extrapolated to pro-
 99 vide an ice-sheet wide correction map for each month.
 100 The same sample of GCMs was selected for monthly ocean surface temper-
 101 ature fields which were bias-corrected against the Extended Reconstructed
 102 Sea Surface Temperature (ERSST) v4 reanalysis product (*Huang et al., 2015*)
 103 using the same methods as for the surface temperature fields. A plot of the
 104 bias for each GCM is provided in the appendix.

105 2.2. Tidewater glaciers

106 A substantial portion of the mass loss of ice sheets and near-polar glaciers
 107 comes from calving (*Rignot and Kanagaratnam, 2006; Benn et al., 2007a;*
 108 *Barrand et al., 2013b*). While the importance of iceberg calving has been
 109 recognised and a number of empirical calving laws have been proposed (*Brown*
 110 *et al., 1982; van der Veen, 1996; Benn et al., 2007b; Alley et al., 2008; Luck-*
 111 *man et al., 2015*), modelling iceberg calving remains a major source of un-
 112 certainty in ice-sheet models (*O’Leary and Christoffersen, 2013*). Unlike

113 the rest of the Antarctic Ice Sheet, the AP is located in a maritime climate,
 114 experiencing significant surface melt during the austral summer. These char-
 115 acteristics, combined with small- to medium-size calving fronts, demonstrate
 116 strong similarity to tidewater glacier systems in Alaska, Svalbard, and coastal
 117 Greenland. In the absence of a universal calving law, a scenario-type ap-
 118 proach was employed utilising three different types of calving criteria which
 119 have been used to successfully simulate calving front retreat in at least one
 120 of these regions (*Brown et al.*, 1982; *van der Veen*, 1996; *Luckman et al.*,
 121 2015). Each calving criterion is assessed in a separate simulation.
 122 The first criterion (henceforth, water depth) relates calving rate to water
 123 depth (e.g *Brown et al.*, 1982), using the updated formula from *Pelto and*
 124 *Warren* (1991)

$$V_c = 70 + 8.33D_w, \quad (1)$$

125 where V_c is the calving rate in $m\ yr^{-1}$ and D_w is the water depth in m at
 126 the calving front.

127 The second criterion (henceforth, flotation criterion) follows *van der Veen*
 128 (1996) who argues that the calving front position is controlled by water depth
 129 and ice thickness, following the relationship:

$$H_c = \frac{\rho_w}{\rho_i} D_w + H_0, \quad (2)$$

130 where H_c is the critical thickness, ρ_w and ρ_i are water and ice densities,
 131 respectively, and H_0 represents the minimum thickness above the flotation
 132 thickness. Based on modelling studies from Columbia Glacier, Alaska (*van der*
 133 *Veen*, 1996), this parameter is set to 50 m in our experiments. Equation 2
 134 does not provide a calving rate, but rather states that if the calving front

135 thickness becomes less than a critical thickness H_c , the calving front becomes
136 unstable and retreats by calving icebergs.
137 Recent studies have highlighted the importance of ocean temperatures and
138 submarine melting to calving (e.g. *Straneo et al.*, 2010; *Luckman et al.*, 2015).
139 *Luckman et al.* (2015) derived a linear relationship between water tempera-
140 ture and calving rate for 3 tidewater glaciers in Svalbard. Due to the climatic
141 similarities between AP glaciers and Svalbard glaciers, the linear law (hence-
142 forth, ocean criterion) was adopted, following the form:

$$V_c = 0.35 \times T, \quad (3)$$

143 where V_c is in m per month and T is the ocean temperature between 20-60 m
144 in °C. Instead of ocean temperatures between 20-60 m, ocean induced calv-
145 ing simulations are forced by monthly ocean surface temperature projections.
146 Ocean surface temperatures do not provide a good predictor for forecasting
147 short term calving trends as these lead frontal ablation by 1-2 months (*Luck-*
148 *man et al.*, 2015). However, since long-term calving behaviour is investigated,
149 using ocean surface temperatures is justified. This is corroborated by a com-
150 parison of mean ocean surface temperatures from the World Ocean Database
151 (*Levitus et al.*, 2013) between 1995-2004 for the model domain with mean
152 ocean temperatures for the same period for depths between 20-60 m. This
153 results in a mean decadal temperature difference of $0.19 \pm 0.18^\circ\text{C}$ between
154 the two data sets. A maximum distance of 100 km between calving front
155 and ocean pixel was selected, resulting in omission of the CSIRO GCM from
156 further analysis.

157

158 2.3. Ice-shelf tributary glaciers

159 In order to model the ice dynamic contribution from ice-shelf tributary
160 glaciers, two important parameters need to be estimated: i) ice-shelf collapse
161 timing and ii) the expected grounding line retreat in response to ice-shelf
162 removal.

163 Ice-shelf collapse timing is computed here according to the total number of
164 melt days in a melt year, a direct link to the physical process of hydrofracture.
165 Several studies noted that immediately prior to the collapse of Larsen B Ice
166 Shelf, the number of melt days and thus the number of observed melt ponds
167 increased dramatically (e.g. *Scambos et al.*, 2003; *van den Broeke*, 2005). A
168 shelf collapse melt day threshold of 102 days was calculated based on obser-
169 vational data from QuikSCAT microwave measurements over Larsen B Ice
170 Shelf (*Barrand et al.*, 2013c), a melt day threshold similar to a range of pre-
171 viously reported values (*Scambos et al.*, 2003; *van den Broeke*, 2005). Future
172 melt days and ice-shelf collapse timing were computed from an ensemble of
173 13 CMIP5 GCM runs (see section Climate data and preprocessing).

174 Ice flux across the grounding line is restrained in the presence of an ice-shelf
175 (*Schoof*, 2007). Following *Gudmundsson* (2013) the normalised buttressing
176 factor is computed:

$$\Theta = \frac{N}{N_0}, \quad (4)$$

177 where N is the normal pressure in presence of an ice-shelf, defined by

$$N = \vec{n}_{gl}^T (R \vec{n}_{gl}). \quad (5)$$

178 N_0 is the ocean pressure acting normal to the grounding when no ice-shelf is
 179 present

$$N_0 = \frac{1}{2}\rho gh \quad (6)$$

180 The vector \vec{n}_{gl} is the unit normal to the grounding line and,

$$R = 2\eta \begin{pmatrix} 2\frac{du}{dx} + \frac{dv}{dy} & \frac{1}{2} \left(\frac{du}{dy} + \frac{dv}{dx} \right) \\ \frac{1}{2} \left(\frac{du}{dy} + \frac{dv}{dx} \right) & 2\frac{dv}{dy} + \frac{du}{dx} \end{pmatrix}, \quad (7)$$

181 where η is the viscosity, $\rho = \rho_i \left(1 - \frac{\rho_i}{\rho_w}\right)$, and h is the ice thickness at the
 182 grounding line.

183 Defined by Equation 4, drainage basins are buttressed when $0 \leq \Theta \leq 1$;
 184 the ice-shelf is actually pulling the grounded ice when $\Theta > 1$; and drainage
 185 basins are overbuttressed when $\Theta < 0$. Overbuttressed (or $\Theta < 0$) means
 186 that ice slows down as it approaches the grounding line, and mass conser-
 187 vation would require that ice thickens towards the grounding line ($\frac{dh}{dx} > 0$).
 188 Θ was computed for each drainage basin using velocity data from *Rignot*
 189 *et al.* (2011), viscosity data from output of an ice-sheet model inversion of
 190 surface velocity data (*Arthern et al.*, 2015), and ice thickness data from *Huss*
 191 *and Farinotti* (2014) where available and Bedmap2 (*Fretwell et al.*, 2013)
 192 elsewhere. 128 of the 215 ice-shelf tributary drainage basins are buttressed,
 193 52 experience ice-shelf pulling, and 35 drainage basins are overbuttressed.
 194 Basins experiencing ice-shelf pulling are characterised by narrow ice fronts
 195 with strong shear margins. These basins are omitted from the analysis as
 196 we do not expect any ice dynamical adjustment following ice-shelf collapse.
 197 While ice dynamical changes may be expected for overbuttressed drainage
 198 basins, these glaciers were also excluded from further analysis as Schoof's

199 flux formula (*Schoof*, 2007, equation 29) is not valid for these cases.
200 The new parameterisation of grounding line retreat is based on the assump-
201 tion that highly buttressed drainage basins will react more to ice-shelf re-
202 moval than lightly buttressed basins. Ice flux across the grounding line is
203 computed for each drainage basin for the buttressed and the unbuttressed
204 case ($\Theta = 1$) using Schoof’s flux formula (*Schoof*, 2007). The remaining
205 input data for Schoof’s flux formula (basal drag and rheological coefficient)
206 were obtained from output of an ice-sheet model inversion (*Arthern et al.*,
207 2015).
208 Adjustment times for drainage basins are scaled to Θ . The maximum mean
209 adjustment time (for infinitesimal positive Θ) is set to 20 years, following
210 observations from Larsen A Ice Shelf (*Rott et al.*, 2014) and no mean ad-
211 justment time is allowed for $\Theta = 1$. In between these bounds, the mean
212 adjustment time is computed using Schoof’s Θ exponent:

$$M \propto \Theta^{\left(\frac{n}{m+1}\right)} \quad (8)$$

213 where M is the mean adjustment time, $n=3$, and $m=1/3$.
214 As mean adjustment times are based on current observations, uncertainties
215 are associated with adjustment times derived from equation 8. To account for
216 this, we allow for uncertainty in the grounding line retreat rates within the
217 bounds of a mean adjustment time. These realisations are set by a gamma
218 distribution with shape parameters $k = M/1.5$ and $\Theta_\gamma = 1.5$. The shape
219 parameters represent greater certainty in short adjustment times and less
220 certainty over longer adjustment timescales, allowing wider spread around
221 the mean adjustment time in the latter case (Figure 1a). For each of the
222 10000 computed adjustment times, a corresponding step-response function

for Θ is computed (Figure 1b). This mimics the behaviour observed in the Amundsen Sea Sector of West Antarctica where glaciers have been observed to retreat rapidly, then remain stable, before rapid retreat commences again (*Favier et al.*, 2014). The number of steps in the function and when these steps occur for each step-response function are randomly determined (Figure 1b). However, the maximum number of steps has to be smaller or equal to the adjustment time. The grounding line retreat for each realisation is then computed as follows:

$$\Delta x_{gl} = \sum_{M=1}^M \frac{(q_{bgl_M} - q_{gl})}{h_{gl}} \quad (9)$$

Here, q_{gl} is the unbuttressed grounding line flux and q_{bgl_M} is the buttressed flux for that year using the updated Θ value from the step-response function (Figure 1b). The retreat distance for each ice-shelf buttressed drainage basin is determined by taking the mean of the 10000 retreat realisations (see Table 1).

Grounding line retreat of >1 km is projected for 22 drainage basins. The vast majority of the drainage basins are expected to show very little retreat. The highest retreat rates are located at drainage basins which are strongly buttressed and possess thick ice at the grounding line. The least retreat in response to ice-shelf collapse is expected for the drainage basins of Larsen B (Scar Inlet) and Larsen C Ice Shelf (Table 1). This is in agreement with independent model simulations suggesting passive shelf ice at Larsen C Ice Shelf (collapse of the shelf will not induce much grounding line retreat at upstream basins (*Fürst et al.*, 2016)).

245 2.4. Model and experimental design

246 Ice dynamic contribution to SLR was simulated with the British Antarctic
247 Survey Antarctic Peninsula Ice Sheet Model (BAS-APISM), previously
248 shown to be suitable for the unique topographic setting of the AP (*Barrand*
249 *et al.*, 2013a; *Schannwell et al.*, 2015). Our simulations comprise two exper-
250 iments: i) the SLR contribution to 2300 of 235 drainage basins is computed,
251 using a range of empirically-based calving criteria. In the first simulation,
252 iceberg calving is allowed until 2100 and in the second simulation, calving is
253 permitted until 2300. Differing forcing periods for calving were applied to in-
254 vestigate their influence on sea-level projections at the end of the simulation
255 period. In experiment ii) the end members of the calving simulation permit-
256 ting calving until 2300 are combined with SLR projections from 215 ice-shelf
257 tributary glaciers to estimate the total ice dynamic SLR contribution for the
258 AP. Ice-shelf collapse is permitted until 2300 for all simulations.

259 3. Results and Discussion

260 3.1. Sea-level rise from tidewater glaciers

261 Simulated SLR projections from tidewater glaciers underline their crucial
262 importance to the regional sea-level budget of the AP region. For the simula-
263 tion allowing calving to 2100, projections are between 3.2 ± 1.6 mm and 18.6
264 mm, and for the experiment permitting calving to 2300 between 8.7 ± 2.9 and
265 18.6 mm. Uncertainty ranges ($\pm 1\sigma$) are available for ocean criterion simula-
266 tions only. Across the two experiments, differences are present in projections
267 from the ocean criterion, indicating a considerable change in ocean forcing
268 between the emission scenarios (Figure 2).

269 Differences in SLR projections are most pronounced in the simulations al-
270 lowing calving to 2100 (Figure 3a). In these simulations, projections from
271 the ocean criterion are an order of magnitude smaller than projections from
272 the flotation and the water depth criteria. These two calving criteria project
273 the vast majority of their total SLR by 2300 over the next 50 years. This
274 is mainly due to the fact that a few drainage basins (e.g. Fleming Glacier,
275 Wordie Bay) rest on bedrock located well below sea level and thus are very
276 vulnerable to iceberg calving in the flotation and water depth criteria (see
277 equations 1 and 2). In contrast to the projected 18.6 and 13.7 mm by 2300
278 from the water depth and flotation criteria respectively, SLR projections us-
279 ing ocean forcing are moderate, projecting 3.2 ± 1.6 mm for the RCP4.5 and
280 5.0 ± 2.3 mm for the RCP8.5 emission scenario (Figure 3a).

281 These differences in SLR projections are smaller in the simulations where
282 iceberg calving is permitted until 2300. While SLR projections from the
283 water depth and flotation criteria remain unchanged, projections from the
284 ocean criterion are an order of magnitude higher and in a very similar range
285 as the other calving criteria (Figure 3b). This means that for the water
286 depth and flotation criteria, all retreat is projected to occur prior to 2100
287 in all simulations. In contrast SLR projections from the ocean criterion are
288 small to 2050 (< 1 mm), but increase dramatically after that. The RCP8.5
289 scenario projects even marginally higher SLR than the flotation criterion at
290 13.9 ± 2.1 mm, while scenario RCP4.5 projects a SLR of 8.7 ± 2.9 mm by 2300
291 (Figure 3b).

292 The larger discrepancy in SLR between the emission scenarios can be ex-
293 plained by the much steeper increase in ocean temperatures for the RCP8.5

294 scenario in the latter two centuries of the simulation period. While there is
295 only a 1.8 ± 0.7 mm difference in the first simulation (Figure 3a), this differ-
296 ence almost triples to 5.2 ± 0.8 mm in the second simulation (Figure 3b). This
297 is also reflected in the ocean temperature projections (Figure 2). In 2100,
298 the temperature difference between the scenarios is at 0.6°C , but increases
299 to 4°C by 2300. The total warming observed in the multi model mean of
300 RCP8.5 is 4.6°C (Figure 2). This ocean warming however is not spatially
301 homogeneous. Rather, there are noticeable differences between the west and
302 east coasts of the peninsula. To the west of the peninsula, warming is more
303 pronounced at 0.96°C per century, compared to 0.85°C for the eastern side
304 of the peninsula. This modelled temperature disparity between the two re-
305 gions continues the pattern observed in the second half of the 20st century
306 (*Meredith and King, 2005*).

307 In the absence of a universal calving law, it is important to note that none
308 of our calving criteria are specifically tuned for the AP. BAS-APISM also
309 cannot simulate glacier front advance. These limitations mean that the SLR
310 numbers reported here should be understood as a first-order estimate of SLR
311 from tidewater glaciers. While surface ocean temperatures appear to be a
312 reasonable approximation of temperatures at depths between 20-60 m, un-
313 certainties remain how well these modelled temperatures reproduce coastal
314 ocean temperatures. The projected 18.6 mm from the water depth criterion
315 should be interpreted as a maximum that can be expected from these 235
316 glaciers. In the simulations using this criterion, the calving front retreats at
317 each drainage basin until the bedrock on which the glacier rests is very close
318 to sea level.

319 Evaluating the suitability of calving criteria to project calving rates remains
 320 difficult. Studies investigating calving behaviour of individual glaciers in dif-
 321 ferent environmental settings have noted that the processes controlling calv-
 322 ing are multi-faceted and may vary for individual glaciers (*Nick et al.*, 2013;
 323 *James et al.*, 2014; *Luckman et al.*, 2015). Other studies have successfully
 324 reproduced calving retreat rates using simple empirical calving criteria (*Vieli*
 325 *et al.*, 2001; *Nick and Oerlemans*, 2006). An indication of the general agree-
 326 ment across the calving criteria is provided by the second simulation (Figure
 327 3b), where Fleming and Prospect glacier, Wordie Bay, are the largest single
 328 contributors to SLR regardless of the applied calving criteria, projected to
 329 contribute between 1.8 - 3.4 mm to SLR by 2300.

330 *3.2. Combined ice dynamical sea-level rise*

331 The combined SLR projections in the RCP4.5 scenario are dominated
 332 by the contributions from tidewater glaciers, accounting between 79% and
 333 89% to the combined SLR. There is a very minor contribution from ice-shelf
 334 tributary glaciers to 2150, and their contribution to 2300 remains small at
 335 2.4 ± 1.5 mm. This relative unimportance is due to the absence of ice-shelf
 336 collapse (Figure 4). In the RCP4.5 scenario, the multi model mean sug-
 337 gests disintegration of 50% of the 10 ice shelves (Figure 4). Only one of the
 338 ice-shelf tributary glaciers of George VI Central contributes significantly to
 339 SLR. This basin is responsible for 67% of the SLR projected from ice-shelf
 340 tributary glaciers, demonstrated by the step in the sea level curve following
 341 this shelf collapse in year 2210 (Figure 5).

342 The overall importance of ice-shelf tributary glaciers to SLR increases in the
 343 RCP8.5 scenario (Figure 5b). All 10 ice-shelves are projected to disintegrate

in this simulation (Figure 4). Moreover, collapse timings of ice-shelves that collapsed in the RCP4.5 occur earlier in RCP8.5. The later the forecasted ice-shelf collapse in RCP4.5, the larger is the shift in timing in the RCP8.5 scenario. While there is only a 33 year shift for Larsen B North, this shift increases to 168 years for George VI North, the last ice-shelf to collapse in the RCP4.5 scenario (Figure 4).

The collapse of more ice-shelves results in much higher SLR projections from ice-shelf tributary glaciers (Figure 4). In contrast to the RCP4.5 scenario, ice-shelf tributary glaciers are as important as tidewater glaciers in this simulation. They contribute 51.4% and 42.4% to the 26.7 ± 16.2 and 32.3 ± 16.2 mm projected for the combined minimum and the combined maximum, respectively (Figure 5b). These projections increase by another 6 ± 1.6 mm if overbuttressed glaciers are taken into account by setting Θ for each of these drainage basins to the minimum value (maximum buttressing) of all ice-shelf tributary glaciers. As overbuttressed drainage basins violate the Schoof flux formula, these projections should be interpreted with caution and are therefore omitted from the total SLR projections. Since not all SLR projections from tidewater glaciers supply uncertainty ranges, uncertainty ranges for all combined SLR projections are reported as $\pm 2\sigma$ of ice-shelf tributary glacier simulations.

The relative importance of each ice-shelf to overall SLR can be assessed from the step size in the SLR curve triggered by individual ice-shelf collapse responses. While some ice-shelf collapses result in no or only a very minor increase in sea level, there are two major steps present in the sea level curve (Figure 5b). These represent the ice-shelves that were identified as the most

369 crucial to overall SLR. By far the largest single contributor to SLR is George
370 VI Ice Shelf South followed by Larsen D Ice Shelf South. The former con-
371 tributes 7.5 ± 4.4 mm by 2300 or 54% of the total contribution from ice-shelf
372 tributary glaciers, while the latter contributes 2 ± 1.6 mm by 2300 or 14% of
373 the total contribution. Combined, these ice-shelves account for 68% of the
374 total projected SLR from ice-shelf tributary glaciers.

375 Ice-shelf collapse is based on an empirical parameterisation of the physi-
376 cal process hypothesised as being the principal reason for ice-shelf collapse
377 - surface meltwater-induced hydrofracture. However, this collapse mecha-
378 nism may not be the sole process driving ice-shelf disintegration (*Shepherd*
379 *et al.*, 2003; *Khazendar et al.*, 2015) and thus ice-shelf collapse might be mis-
380 forecasted. Grounding line retreat from a gradual loss of buttressing (e.g.
381 through ice-shelf thinning) where no collapse occurs was also omitted. More-
382 over, bedrock topography is only taken into account for tidewater glacier
383 retreat computations, omitting the potential of marine-ice-sheet instability
384 (MISI), a self-sustained retreat of the grounding line on retrograde sloping
385 bedrock, in ice-shelf tributary drainage basins. While a recent study sug-
386 gests that widespread MISI is unlikely in the AP (*Ritz et al.*, 2015), there
387 is evidence that some regions might be susceptible to this mechanism (e.g.
388 Scar Inlet and George VI Ice Shelf) (*Farinotti et al.*, 2014; *Wouters et al.*,
389 2015). Despite these simplifications, the implemented grounding line retreat
390 parameterisation predicts plausible retreat rates in agreement with theoret-
391 ical considerations.

392 In comparison to earlier ice dynamical SLR projections from ice-shelf tribu-
393 tary drainage basins by *Schannwell et al.* (2015), the projections presented

here are slightly higher for the RCP4.5 scenario and slightly lower for the RCP8.5 scenario. Discrepancies in SLR between *Schannwell et al.* (2015) and this study arise due to the improvement in grounding line retreat and ice-shelf collapse parameterisations here. Unlike in the previous grounding line retreat parameterisation, the new parameterisation permits estimation of uncertainty ranges for each simulation. Moreover, ice-shelf collapse timing is calibrated on observations, providing a more robust approximation for future collapse estimates.

3.3. Uncertainty assessment

In order to test the robustness of the modelled SLR projections a suite of sensitivity experiments was performed. Since SLR projections from tidewater glaciers should be understood as a first-order estimate and the three calving criteria provide an envelope of future scenarios, the sensitivity experiments concentrate on ice-shelf tributary SLR contributions.

There are two main sources of uncertainty: climate (ice-shelf collapse timing) and grounding line retreat parameterisation. The influence of climate variability on SLR projections is demonstrated by the difference between the two emission scenarios. In RCP8.5, projections are ~ 6 fold higher than in RCP4.5. Nonetheless, the importance of ice-shelf collapse timing in a worst-case scenario is relatively moderate. The most extreme scenario with immediate collapse of all fringing ice-shelves leads to an increase of 3.7 mm (27%) in comparison to the projection from RCP8.5.

How much the position of the grounding line changes in response to ice-shelf collapse is of crucial importance for SLR projections from ice-shelf tributary

419 glaciers. In the parameterisation implemented here, the mean adjustment
420 time is scaled to buttressing and is based on available observations from
421 Larsen A Ice Shelf. Since ice dynamical changes are still ongoing in this
422 area, maximum adjustment time might be underestimated. Grounding line
423 retreat rates for each basin were computed using Schoof’s flux formula. To
424 investigate the sensitivity of the results, key parameters such as adjustment
425 time and all input data to the flux formula were perturbed by $\pm 20\%$. Re-
426 sults show that by far the most important parameter is ice thickness at the
427 grounding line. SLR projections from all other perturbed parameters vary by
428 $< 46\%$ ($< 4.7 \pm 1.7$ mm) in comparison to the reference simulations and lie all
429 within the reported uncertainty ranges. For perturbed ice thicknesses how-
430 ever, SLR projections vary by up to $\sim 400\%$ (53.2 ± 16.6 mm), increasing SLR
431 projections in RCP8.5 to 66.9 ± 25 mm, more than double the SLR projected
432 for the combined RCP8.5 reference simulation. These results highlight the
433 key importance of accurate estimates of ice thickness at glacier grounding
434 lines.

435 To investigate the robustness of the results to perturbations to ice velocity,
436 the velocity map was perturbed by adding normally distributed noise ($\sigma =$
437 1 SD of unperturbed velocity map) to the unperturbed velocity map. Ice
438 velocity was used to estimate buttressing at each drainage basin. The per-
439 turbed velocity map was used to compute new Θ values for the 128 modelled
440 drainage basins. Of the 128 normally buttressed basins in the reference simu-
441 lation, 26 change to being overbuttressed and 31 to being unbuttressed. This
442 leaves 71 drainage basins for the perturbed model simulation. Despite the
443 smaller number of drainage basins, change in SLR for the RCP8.5 scenario

444 is negligible ($\sim 1\%$) in comparison to the reference simulation, indicating an
445 increase in buttressing for these 70 drainage basins. Average buttressing for
446 these basins increases from 0.59 to 0.43, negating the effect of fewer drainage
447 basins modelled.

448

449 4. Conclusions

450 This paper has presented the first comprehensive modelling study of SLR
451 projections from both tidewater and ice-shelf tributary glaciers of the AP.
452 In total, the ice dynamical response of 450 drainage basins, comprising 77%
453 of the AP's area, was computed. Tidewater glaciers are an important con-
454 tributor to the ice dynamic SLR projections from the AP. Omission of tide-
455 water glaciers leads to an underestimation of SLR by $>50\%$. In the RCP4.5
456 scenario, SLR projections are dominated by tidewater glaciers contributing
457 $>75\%$ of the combined SLR, while tidewater and ice-shelf tributary glaciers
458 contribute about the same to total SLR in the RCP8.5 scenario. If all ice-
459 shelves disintegrate, George VI Ice Shelf is the largest single contributor,
460 accounting for 9.8 ± 5.5 mm (70%) of the total SLR projected from ice-shelf
461 tributary glaciers. This agrees well with an earlier modelling study (*Schan-*
462 *nwell et al.*, 2015) and is consistent with present-day observations of AP
463 ice-sheet mass balance (*Wouters et al.*, 2015).

464 Sensitivity results show uncertainties in SLR projections remain due to calv-
465 ing, ice-shelf collapse, and grounding line retreat parameterisation. SLR
466 projections for ice-shelf tributary glaciers are highly sensitive to ice thickness
467 and to a lesser extent ice velocity. To reduce uncertainties further in future

468 simulations, accurate ice thickness and velocity maps are required for com-
 469 putation of buttressing and ice flux across the grounding line.
 470 The Antarctic Peninsula Ice Sheet is projected to contribute between 11 ± 2
 471 and 32 ± 16 mm to global SLR by 2300, depending on emission scenario. This
 472 corresponds to an annual contribution of 0.04 ± 0.01 mm a⁻¹ and 0.11 ± 0.05
 473 mm a⁻¹ over the next three centuries, respectively. For comparison, the
 474 SLR contribution from the entire Antarctic Ice Sheet derived from satel-
 475 lite observations between 2003-2013 was 0.25 ± 0.07 mm a⁻¹ (*Martín-Español*
 476 *et al.*, 2016). These findings underline the continued importance of ice dy-
 477 namic SLR from the AP, even though the AP comprises only 1% of the total
 478 Antarctic Ice Sheet area.

479 Acknowledgements

480 C.S. was supported by a PhD studentship from the University of Birm-
 481 ingham. The computations described in this paper were performed using
 482 the University of Birmingham BlueBEAR HPC service, which provides a
 483 High Performance Computing service to the University’s research community.
 484 See <http://www.birmingham.ac.uk/bear> for more details. We acknowledge
 485 the World Climate Research Programmes Working Group on Coupled Mod-
 486 elling, which is responsible for CMIP, and we thank the climate modeling
 487 groups for producing and making available their model output (available at
 488 <http://pcmdi9.llnl.gov/>). For CMIP the U.S. Department of Energys Pro-
 489 gram for Climate Model Diagnosis and Intercomparison provides coordinat-
 490 ing support and led development of software infrastructure in partnership
 491 with the Global Organization for Earth System Science Portals. We also

492 thank Rob Arthern for fruitful discussions and for providing model output
493 data for our computations.

494 **References**

- 495 Alley, R. B., H. J. Horgan, I. Joughin, K. M. Cuffey, T. K. Dupont, B. R.
496 Parizek, S. Anandakrishnan, and J. Bassis (2008), A simple law for ice-shelf
497 calving, *Science*, *322*(5906), 1344–1344, doi:10.1126/science.1162543.
- 498 Arthern, R. J., R. C. A. Hindmarsh, and C. R. Williams (2015), Flow speed
499 within the Antarctic ice sheet and its controls inferred from satellite ob-
500 servations, *Journal of Geophysical Research: Earth Surface*, *120*(7), 1171–
501 1188, doi:10.1002/2014JF003239.
- 502 Barrand, N. E., R. C. A. Hindmarsh, R. J. Arthern, C. R. Williams,
503 J. Mouginot, B. Scheuchl, E. Rignot, S. R. M. Ligtenberg, M. R. Van
504 Den Broeke, T. L. Edwards, A. J. Cook, and S. B. Simonsen (2013a),
505 Computing the volume response of the Antarctic Peninsula ice sheet to
506 warming scenarios to 2200, *Journal of Glaciology*, *59*(215), 397–409, doi:
507 10.3189/2013JoG12J139.
- 508 Barrand, N. E., H. Machguth, and J. O. Hagen (2013b), Observing changes
509 in near-polar glaciers in the northern and southern hemispheres, *Eos*,
510 *Transactions American Geophysical Union*, *94*(23), 208–208, doi:10.1002/
511 2013EO230007.
- 512 Barrand, N. E., D. G. Vaughan, N. Steiner, M. Tedesco, P. Kuipers Munneke,
513 M. R. van den Broeke, and J. S. Hosking (2013c), Trends in Antarctic
514 Peninsula surface melting conditions from observations and regional cli-
515 mate modeling, *Journal of Geophysical Research: Earth Surface*, *118*(1),
516 315–330, doi:10.1029/2012JF002559.

- 517 Benn, D. I., C. R. Warren, and R. H. Mottram (2007a), Calving processes and
 518 the dynamics of calving glaciers, *Earth-Science Reviews*, *82*(3-4), 143–179,
 519 doi:http://dx.doi.org/10.1016/j.earscirev.2007.02.002.
- 520 Benn, D. I., N. R. J. Hulton, and R. H. Mottram (2007b), 'Calving laws',
 521 'sliding laws' and the stability of tidewater glaciers, *Annals of Glaciology*,
 522 *46*(1), 123–130, doi:10.3189/172756407782871161.
- 523 Borstad, C., A. Khazendar, B. Scheuchl, M. Morlighem, E. Larour, and
 524 E. Rignot (2016), A constitutive framework for predicting weakening and
 525 reduced buttressing of ice shelves based on observations of the progres-
 526 sive deterioration of the remnant Larsen B Ice Shelf, *Geophysical Research*
 527 *Letters*, *43*(5), 2015GL067,365, doi:10.1002/2015GL067365.
- 528 Brown, C. S., M. F. Meier, and A. Post (1982), Calving speed of Alaska tide-
 529 water glaciers, with application to Columbia Glacier, *USGS Professional*
 530 *Paper*, *1258-C*, C1–C13.
- 531 Cook, A. J., A. J. Fox, D. G. Vaughan, and J. G. Ferrigno (2005), Retreat-
 532 ing glacier fronts on the Antarctic Peninsula over the past half-century,
 533 *Science*, *308*(5721), 541–544, doi:10.1126/science.1104235.
- 534 Dee, D. P., S. M. Uppala, A. J. Simmons, P. Berrisford, P. Poli, S. Kobayashi,
 535 U. Andrae, M. A. Balmaseda, G. Balsamo, P. Bauer, P. Bechtold, A. C. M.
 536 Beljaars, L. van de Berg, J. Bidlot, N. Bormann, C. Delsol, R. Dragani,
 537 M. Fuentes, A. J. Geer, L. Haimberger, S. B. Healy, H. Hersbach, E. V.
 538 Hólm, L. Isaksen, P. Kållberg, M. Köhler, M. Matricardi, A. P. McNally,
 539 B. M. Monge-Sanz, J. J. Morcrette, B. K. Park, C. Peubey, P. de Rosnay,

- 540 C. Tavorato, J. N. Thépaut, and F. Vitart (2011), The ERA-Interim re-
 541 analysis: Configuration and performance of the data assimilation system,
 542 *Quarterly Journal of the Royal Meteorological Society*, *137*(656), 553–597,
 543 doi:10.1002/qj.828.
- 544 Farinotti, D., E. C. King, A. Albrecht, M. Huss, and G. H. Gudmundsson
 545 (2014), The bedrock topography of Starbuck Glacier, Antarctic Penin-
 546 sula, as determined by radio-echo soundings and flow modeling, *Annals of*
 547 *Glaciology*, *55*(67), 22–28, doi:doi:10.3189/2014AoG67A025.
- 548 Favier, L., G. Durand, S. L. Cornford, G. H. Gudmundsson,
 549 O. Gagliardini, F. Gillet-Chaulet, T. Zwinger, A. J. Payne, and
 550 A. M. Le Brocq (2014), Retreat of Pine Island Glacier controlled
 551 by marine ice-sheet instability, *Nature Clim. Change*, *4*(2), 117–
 552 121, doi:10.1038/nclimate2094[http://www.nature.com/nclimate/journal/](http://www.nature.com/nclimate/journal/v4/n2/abs/nclimate2094.html#supplementary-information)
 553 [v4/n2/abs/nclimate2094.html#supplementary-information](http://www.nature.com/nclimate/journal/v4/n2/abs/nclimate2094.html#supplementary-information).
- 554 Fretwell, P., H. D. Pritchard, D. G. Vaughan, J. L. Bamber, N. E. Bar-
 555 rand, R. Bell, C. Bianchi, R. G. Bingham, D. D. Blankenship, G. Casassa,
 556 G. Catania, D. Callens, H. Conway, A. J. Cook, H. F. J. Corr, D. Damaske,
 557 V. Damm, F. Ferraccioli, R. Forsberg, S. Fujita, Y. Gim, P. Gogineni,
 558 J. A. Griggs, R. C. A. Hindmarsh, P. Holmlund, J. W. Holt, R. W. Ja-
 559 cobel, A. Jenkins, W. Jokat, T. Jordan, E. C. King, J. Kohler, W. Kra-
 560 bill, M. Riger-Kusk, K. A. Langley, G. Leitchenkov, C. Leuschen, B. P.
 561 Luyendyk, K. Matsuoka, J. Mouginot, F. O. Nitsche, Y. Nogi, O. A. Nost,
 562 S. V. Popov, E. Rignot, D. M. Rippin, A. Rivera, J. Roberts, N. Ross,
 563 M. J. Siegert, A. M. Smith, D. Steinhage, M. Studinger, B. Sun, B. K.

564 Tinto, B. C. Welch, D. Wilson, D. A. Young, C. Xiangbin, and A. Ziriz-
565 zotti (2013), Bedmap2: improved ice bed, surface and thickness datasets
566 for antarctica, *The Cryosphere*, 7(1), 375–393, doi:10.5194/tc-7-375-2013,
567 tC.

568 Fürst, J. J., G. Durand, F. Gillet-Chaulet, L. Tavad, M. Rankl,
569 M. Braun, and O. Gagliardini (2016), The safety band of Antarc-
570 tic ice shelves, *Nature Clim. Change*, *advance online publica-*
571 *tion*, doi:10.1038/nclimate2912[http://www.nature.com/nclimate/journal/](http://www.nature.com/nclimate/journal/vaop/ncurrent/abs/nclimate2912.html#supplementary-information)
572 [vaop/ncurrent/abs/nclimate2912.html#supplementary-information](http://www.nature.com/nclimate/journal/vaop/ncurrent/abs/nclimate2912.html#supplementary-information).

573 Gudmundsson, G. H. (2013), Ice-shelf buttressing and the stability of marine
574 ice sheets, *The Cryosphere*, 7(2), 647–655, doi:10.5194/tc-7-647-2013, tC.

575 Holland, P. R., A. Brisbourne, H. F. J. Corr, D. McGrath, K. Purdon,
576 J. Paden, H. A. Fricker, F. S. Paolo, and A. H. Fleming (2015), Oceanic
577 and atmospheric forcing of Larsen C Ice-Shelf thinning, *The Cryosphere*,
578 9(3), 1005–1024, doi:10.5194/tc-9-1005-2015.

579 Huang, B., V. F. Banzon, E. Freeman, J. Lawrimore, W. Liu, T. C. Peterson,
580 T. M. Smith, P. W. Thorne, S. D. Woodruff, and H.-M. Zhang (2015),
581 Extended Reconstructed Sea Surface Temperature Version 4 (ERSST.v4).
582 Part I: Upgrades and intercomparisons, *Journal of Climate*, 28(3), 911–
583 930, doi:10.1175/JCLI-D-14-00006.1.

584 Huss, M., and D. Farinotti (2014), A high-resolution bedrock map for
585 the Antarctic Peninsula, *The Cryosphere*, 8(4), 1261–1273, doi:10.5194/
586 tc-8-1261-2014, tC.

James, T. D., T. Murray, N. Selmes, K. Scharrer, and M. O’leary
 (2014), Buoyant flexure and basal crevassing in dynamic mass
 loss at Helheim Glacier, *Nature Geosci*, 7(8), 593–596, doi:
 10.1038/ngeo2204[http://www.nature.com/ngeo/journal/v7/n8/abs/
 ngeo2204.html#supplementary-information](http://www.nature.com/ngeo/journal/v7/n8/abs/ngeo2204.html#supplementary-information), [rsquor].

Jones, P. D., and D. H. Lister (2014), Antarctic near-surface air temperatures
 compared with ERA-Interim values since 1979, *International Journal of
 Climatology*, 35(7), 1354–1366, doi:10.1002/joc.4061.

Khazendar, A., C. P. Borstad, B. Scheuchl, E. Rignot, and H. Seroussi (2015),
 The evolving instability of the remnant Larsen B Ice Shelf and its tributary
 glaciers, *Earth and Planetary Science Letters*, 419, 199–210, doi:[http://dx.
 doi.org/10.1016/j.epsl.2015.03.014](http://dx.doi.org/10.1016/j.epsl.2015.03.014).

Levitus, S., J. Antonov, O. K. Baranova, T. Boyer, C. Coleman, H. Gar-
 cia, A. Grodsky, D. Johnson, R. Locarnini, A. V. Mishonov, C. O’Brien,
 J. Reagan, D. Seidov, I. Smolyar, and M. Zweng (2013), The world ocean
 database, *Data Science Journal*, 12(0), WDS229–WDS234.

Luckman, A., D. I. Benn, F. Cottier, S. Bevan, F. Nilsen, and M. Inall (2015),
 Calving rates at tidewater glaciers vary strongly with ocean temperature,
Nat Commun, 6, doi:10.1038/ncomms9566.

Martín-Español, A., A. Zammit-Mangion, P. J. Clarke, T. Flament, V. Helm,
 M. A. King, S. B. Luthcke, E. Petrie, F. Rémy, N. Schön, B. Wouters, and
 J. L. Bamber (2016), Spatial and temporal Antarctic ice sheet mass trends,
 glacio-isostatic adjustment, and surface processes from a joint inversion

610 of satellite altimeter, gravity, and GPS data, *Journal of Geophysical Re-*
611 *search: Earth Surface*, pp. 1–18, doi:10.1002/2015JF003550.

612 McMillan, M., A. Shepherd, A. Sundal, K. Briggs, A. Muir, A. Rid-
613 out, A. Hogg, and D. Wingham (2014), Increased ice losses from
614 Antarctica detected by CryoSat-2, *Geophysical Research Letters*, *41*(11),
615 2014GL060,111, doi:10.1002/2014GL060111.

616 Meredith, M. P., and J. C. King (2005), Rapid climate change in the
617 ocean west of the Antarctic Peninsula during the second half of the
618 20th century, *Geophysical Research Letters*, *32*(19), L19,604, doi:10.1029/
619 2005GL024042.

620 Nick, F. M., and J. Oerlemans (2006), Dynamics of tidewater glaciers: Com-
621 parison of three models, *Journal of Glaciology*, *52*(177), 183–190, doi:
622 10.3189/172756506781828755.

623 Nick, F. M., A. Vieli, M. L. Andersen, I. Joughin, A. Payne, T. L. Edwards,
624 F. Pattyn, and R. S. W. van de Wal (2013), Future sea-level rise from
625 Greenland’s main outlet glaciers in a warming climate, *Nature*, *497*(7448),
626 235–238, doi:10.1038/nature12068[http://www.nature.com/nature/](http://www.nature.com/nature/journal/v497/n7448/abs/nature12068.html#supplementary-information)
627 [journal/v497/n7448/abs/nature12068.html#supplementary-information](http://www.nature.com/nature/journal/v497/n7448/abs/nature12068.html#supplementary-information).

628 O’Leary, M., and P. Christoffersen (2013), Calving on tidewater glaciers am-
629 plified by submarine frontal melting, *The Cryosphere*, *7*(1), 119–128, doi:
630 10.5194/tc-7-119-2013, tC.

631 Pelto, M. S., and C. R. Warren (1991), Relationship between tidewater glacier

- 632 calving velocity and water depth at the calving front, *Annals of Glaciology*,
633 15, 115–118.
- 634 Pritchard, H. D., and D. G. Vaughan (2007), Widespread acceleration of
635 tidewater glaciers on the Antarctic Peninsula, *Journal of Geophysical Re-*
636 *search: Earth Surface*, 112(F3), n/a–n/a, doi:10.1029/2006JF000597.
- 637 Pritchard, H. D., S. R. M. Ligtenberg, H. A. Fricker, D. G.
638 Vaughan, M. R. van den Broeke, and L. Padman (2012), Antarc-
639 tic ice-sheet loss driven by basal melting of ice shelves, *Nature*,
640 484(7395), 502–505, doi:http://www.nature.com/nature/journal/v484/
641 n7395/abs/nature10968.html, 10.1038/nature10968.
- 642 Radić, V., A. Bliss, A. C. Beedlow, R. Hock, E. Miles, and J. G. Cog-
643 ley (2014), Regional and global projections of twenty-first century glacier
644 mass changes in response to climate scenarios from global climate models,
645 *Climate Dynamics*, 42(1-2), 37–58, doi:10.1007/s00382-013-1719-7.
- 646 Rignot, E., and P. Kanagaratnam (2006), Changes in the velocity structure of
647 the Greenland ice sheet, *Science*, 311(5763), 986–990, doi:10.1126/science.
648 1121381.
- 649 Rignot, E., G. Casassa, P. Gogineni, W. Krabill, A. Rivera, and R. Thomas
650 (2004), Accelerated ice discharge from the Antarctic Peninsula following
651 the collapse of Larsen B ice shelf, *Geophysical Research Letters*, 31(18),
652 L18,401, doi:10.1029/2004GL020697.
- 653 Rignot, E., J. Mouginot, and B. Scheuchl (2011), Ice flow of the Antarctic
654 ice sheet, *Science*, 333(6048), 1427–1430, doi:10.1126/science.1208336.

- 655 Ritz, C., T. L. Edwards, G. Durand, A. J. Payne, V. Peyaud, and R. C. A.
656 Hindmarsh (2015), Potential sea-level rise from Antarctic ice-sheet
657 instability constrained by observations, *Nature*, 528(7580), 115–118,
658 doi:10.1038/nature16147[http://www.nature.com/nature/journal/v528/](http://www.nature.com/nature/journal/v528/n7580/abs/nature16147.html#supplementary-information)
659 [n7580/abs/nature16147.html#supplementary-information](http://www.nature.com/nature/journal/v528/n7580/abs/nature16147.html#supplementary-information).
- 660 Rott, H., W. Rack, P. Skvarca, and H. De Angelis (2002), Northern Larsen
661 Ice Shelf, Antarctica: Further retreat after collapse, *Annals of Glaciology*,
662 34(1), 277–282, doi:10.3189/172756402781817716.
- 663 Rott, H., D. Floricioiu, J. Wuite, S. Scheiblauer, T. Nagler, and M. Kern
664 (2014), Mass changes of outlet glaciers along the Nordensjököld Coast,
665 northern Antarctic Peninsula, based on TanDEM-X satellite measure-
666 ments, *Geophysical Research Letters*, p. 2014GL061613, doi:10.1002/
667 2014GL061613.
- 668 Scambos, T., C. Hulbe, and M. Fahnestock (2003), *Climate-Induced Ice Shelf*
669 *Disintegration in the Antarctic Peninsula*, pp. 79–92, American Geophys-
670 ical Union, doi:10.1029/AR079p0079.
- 671 Scambos, T. A., C. Hulbe, M. Fahnestock, and J. Bohlander (2000),
672 The link between climate warming and break-up of ice shelves in the
673 Antarctic Peninsula, *Journal of Glaciology*, 46(154), 516–530, doi:10.3189/
674 172756500781833043.
- 675 Scambos, T. A., J. A. Bohlander, C. A. Shuman, and P. Skvarca (2004),
676 Glacier acceleration and thinning after ice shelf collapse in the Larsen B

- embayment, Antarctica, *Geophysical Research Letters*, 31(18), n/a–n/a,
doi:10.1029/2004GL020670.
- Scambos, T. A., E. Berthier, T. Haran, C. A. Shuman, A. J. Cook, S. R. M.
Ligtenberg, and J. Bohlander (2014), Detailed ice loss pattern in the north-
ern Antarctic Peninsula: Widespread decline driven by ice front retreats,
The Cryosphere, 8(6), 2135–2145, doi:10.5194/tc-8-2135-2014, tC.
- Schannwell, C., N. E. Barrand, and V. Radić (2015), Modeling ice dynamic
contributions to sea level rise from the Antarctic Peninsula, *Journal of
Geophysical Research: Earth Surface*, 120(11), 2374–2392, doi:10.1002/
2015JF003667.
- Schoof, C. (2007), Ice sheet grounding line dynamics: Steady states, stability,
and hysteresis, *Journal of Geophysical Research: Earth Surface*, 112(F3),
F03S28, doi:10.1029/2006JF000664.
- Shepherd, A., D. Wingham, T. Payne, and P. Skvarca (2003), Larsen Ice
Shelf has progressively thinned, *Science*, 302(5646), 856–859, doi:10.1126/
science.1089768.
- Straneo, F., G. S. Hamilton, D. A. Sutherland, L. A. Stearns, F. Davidson,
M. O. Hammill, G. B. Stenson, and A. Rosing-Asvid (2010), Rapid circula-
tion of warm subtropical waters in a major glacial fjord in East Greenland,
Nature Geosci, 3(3), 182–186, doi:http://www.nature.com/ngeo/journal/
v3/n3/supinfo/ngeo764_S1.html, 10.1038/ngeo764.
- Taylor, K. E., R. J. Stouffer, and G. A. Meehl (2011), An overview of CMIP5

699 and the experiment design, *Bulletin of the American Meteorological Soci-*
700 *ety*, *93*(4), 485–498, doi:10.1175/BAMS-D-11-00094.1.

701 van den Broeke, M. (2005), Strong surface melting preceded collapse
702 of Antarctic Peninsula ice shelf, *Geophysical Research Letters*, *32*(12),
703 L12,815, doi:10.1029/2005GL023247.

704 van der Veen, C. J. (1996), Tidewater calving, *Journal of Glaciology*, *42*(141),
705 375–385.

706 Vaughan, D., G. Marshall, W. Connolley, C. Parkinson, R. Mulvaney,
707 D. Hodgson, J. King, C. Pudsey, and J. Turner (2003), Recent rapid
708 regional climate warming on the Antarctic Peninsula, *Climatic Change*,
709 *60*(3), 243–274, doi:10.1023/A:1026021217991.

710 Vaughan, D. G., and C. S. M. Doake (1996), Recent atmospheric warming
711 and retreat of ice shelves on the Antarctic Peninsula, *Nature*, *379*(6563),
712 328–331, 10.1038/379328a0.

713 Vieli, A., M. Funk, and H. Blatter (2001), Flow dynamics of tidewater
714 glaciers: A numerical modelling approach, *Journal of Glaciology*, *47*(159),
715 595–606, doi:10.3189/172756501781831747.

716 Vuuren, D. P., J. Edmonds, M. Kainuma, K. Riahi, A. Thomson, K. Hib-
717 bard, G. C. Hurtt, T. Kram, V. Krey, J.-F. Lamarque, T. Masui, M. Mein-
718 shausen, N. Nakicenovic, S. J. Smith, and S. K. Rose (2011), The repre-
719 sentative concentration pathways: An overview, *Climatic Change*, *109*(1),
720 5–31, doi:10.1007/s10584-011-0148-z.

721 Wouters, B., A. Martín-Español, V. Helm, T. Flament, J. M. van Wessem,
722 S. R. M. Ligtenberg, M. R. van den Broeke, and J. L. Bamber (2015),
723 Dynamic thinning of glaciers on the southern Antarctic Peninsula, *Science*,
724 348(6237), 899–903, doi:10.1126/science.aaa5727.

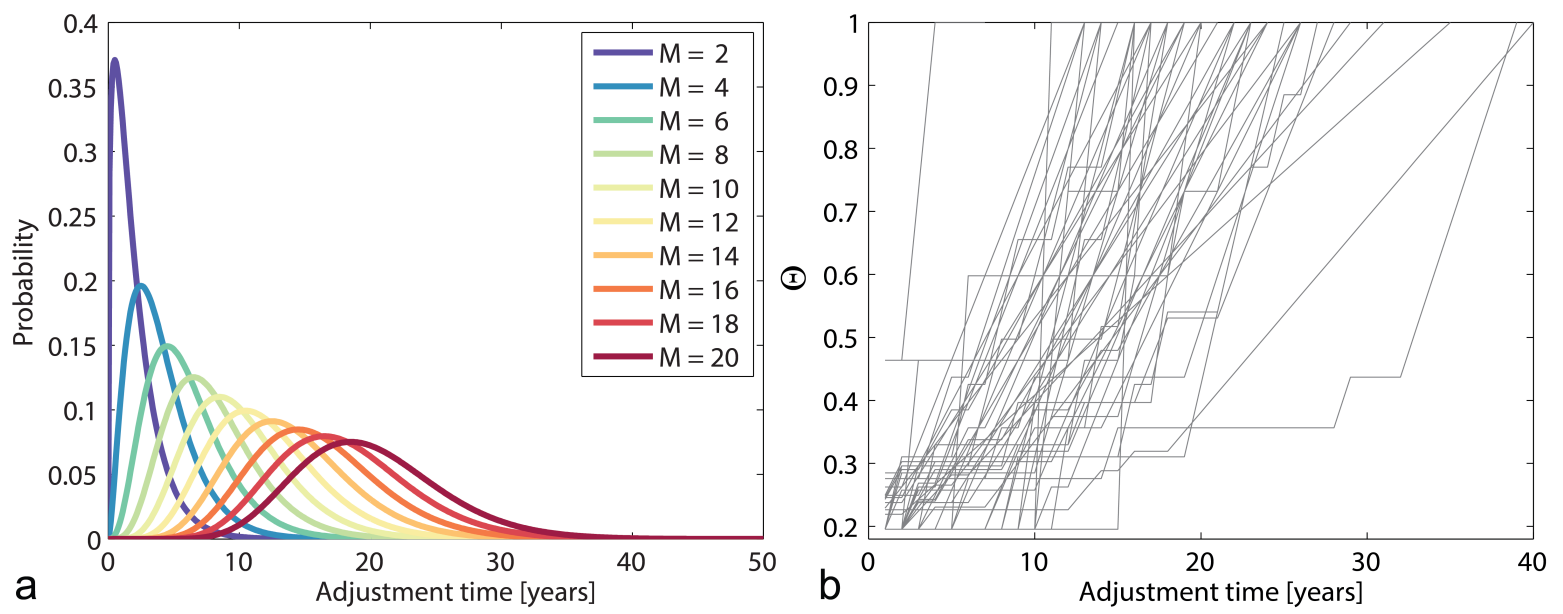


Figure 1: (a) Gamma distributions used in grounding line retreat parameterisation for different mean adjustment times (M). (b) Sample of 100 random step-response functions for corresponding $M = 20$ curve in (a).

Ice-Shelf	Mean Retreat [m]	Θ	No. of basins
Larsen B	691	0.47	6
Larsen C North	405	0.40	17
Larsen C South	215	0.59	31
Larsen D North	656	0.60	16
Larsen D Central	250	0.57	11
Larsen D South	4140	0.66	20
George VI North	1960	0.52	4
George VI Central	7310	0.69	3
George VI South	10530	0.69	8
Stange	29540	0.54	1

Table 1: Ice-shelf grounding line retreat distances, mean buttressing factor (Θ), and the number of basins for each ice-shelf entity.

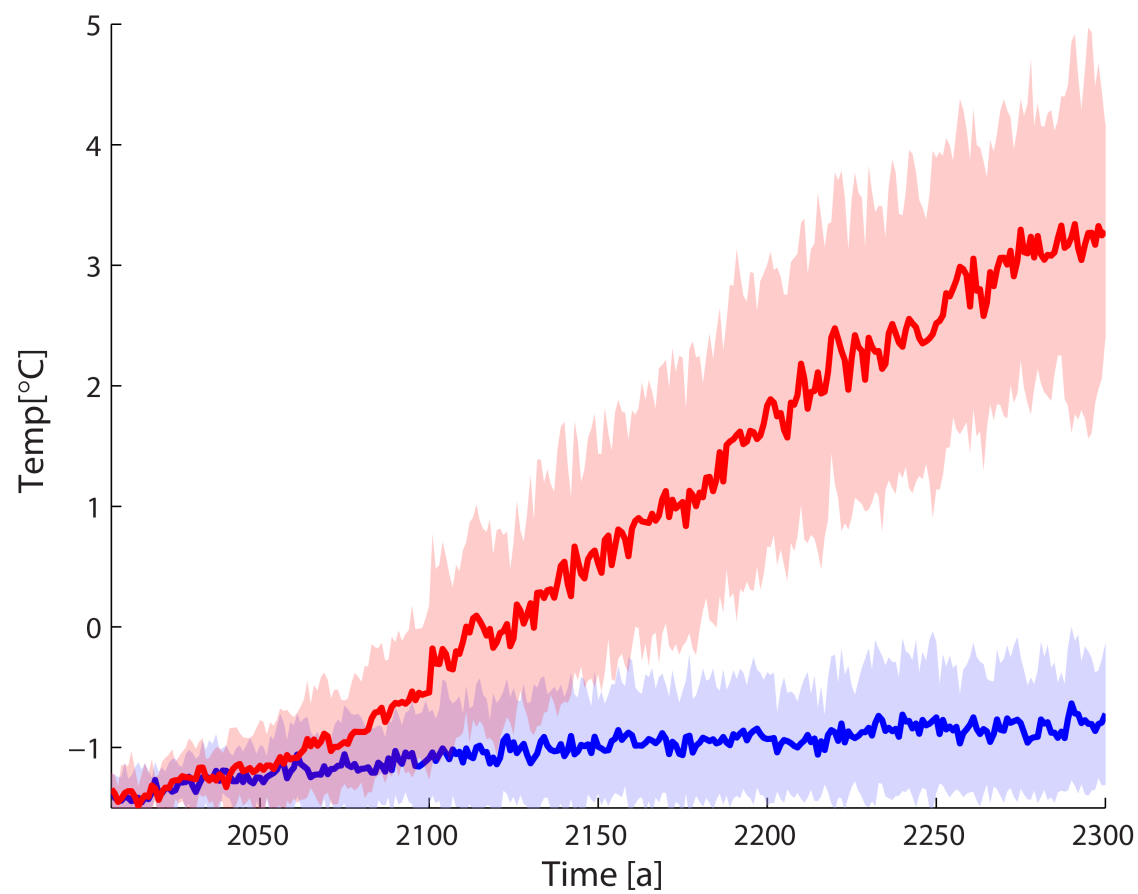


Figure 2: Multi model mean ocean temperatures for the ice-sheet model domain for RCP4.5 (blue line) and RCP8.5 (red line). Shading shows ($\pm 1\sigma$) uncertainty.

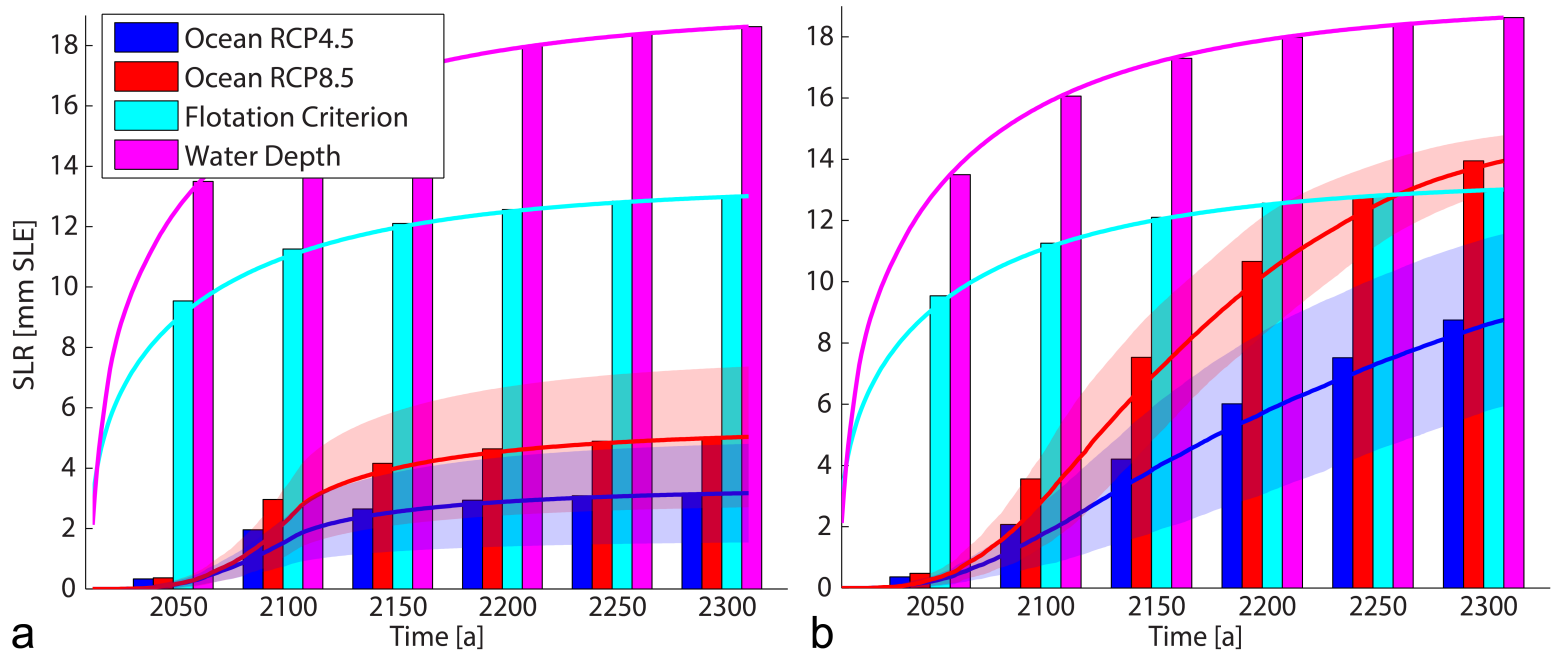


Figure 3: SLR projection from tidewater glaciers permitting calving front retreat to 2100 (a) and to 2300 (b). Shading shows ($\pm 1\sigma$) uncertainty.

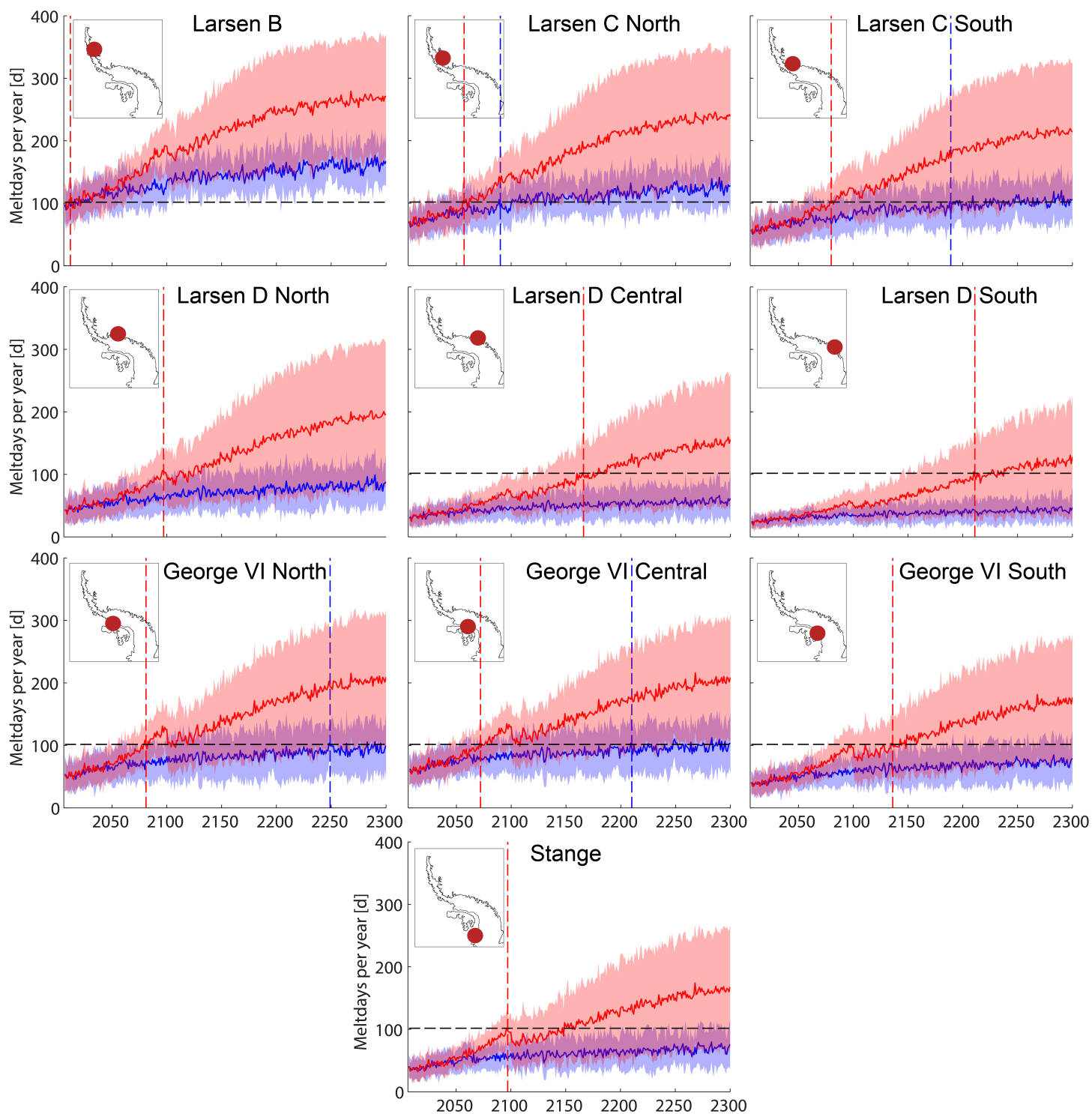


Figure 4: Multi model mean melt day projections for all ice-shelves for the RCP4.5 (solid blue line) and RCP8.5 (solid red line) scenarios. Shading shows ($\pm 1\sigma$) uncertainty. Dashed blue lines and dashed red lines denote ice-shelf collapse timing for the RCP4.5 and RCP8.5 scenarios, respectively. Dashed black line approximates collapse threshold. Note that for Scar Inlet collapse timing for both scenarios is forecasted for the same year.

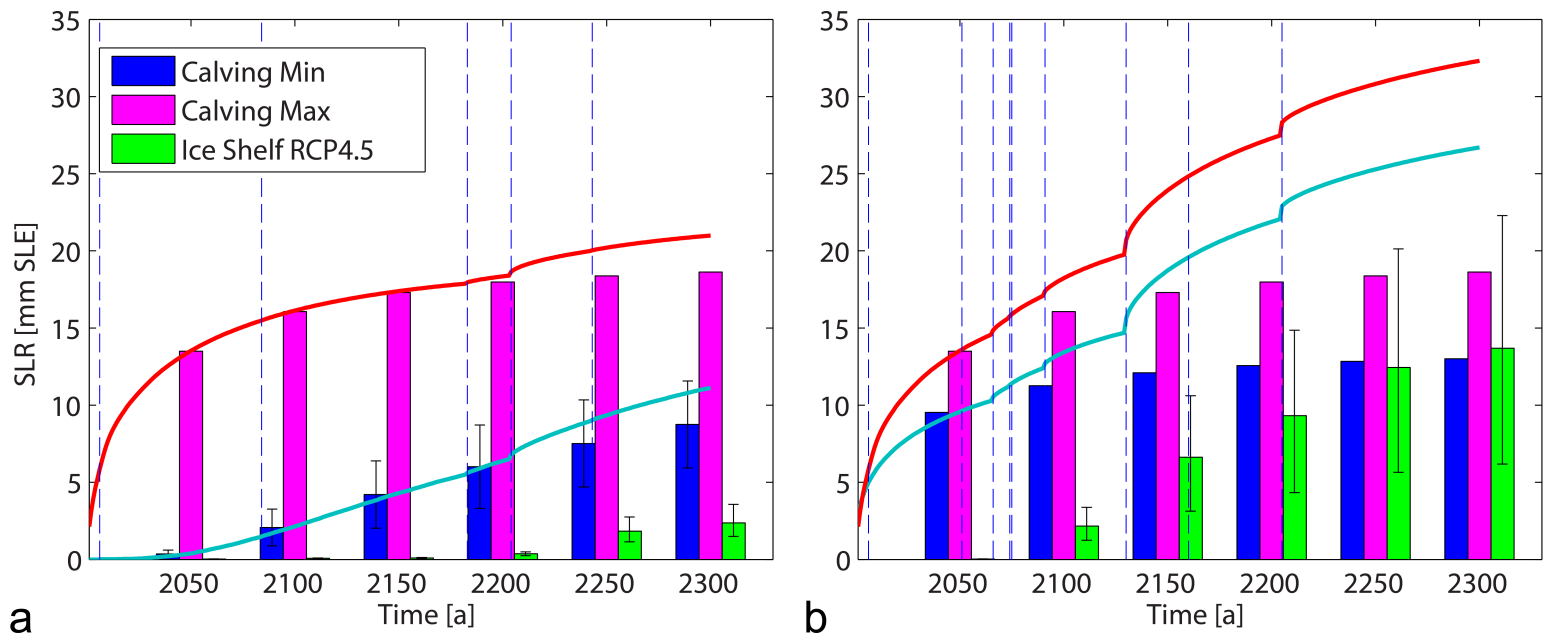
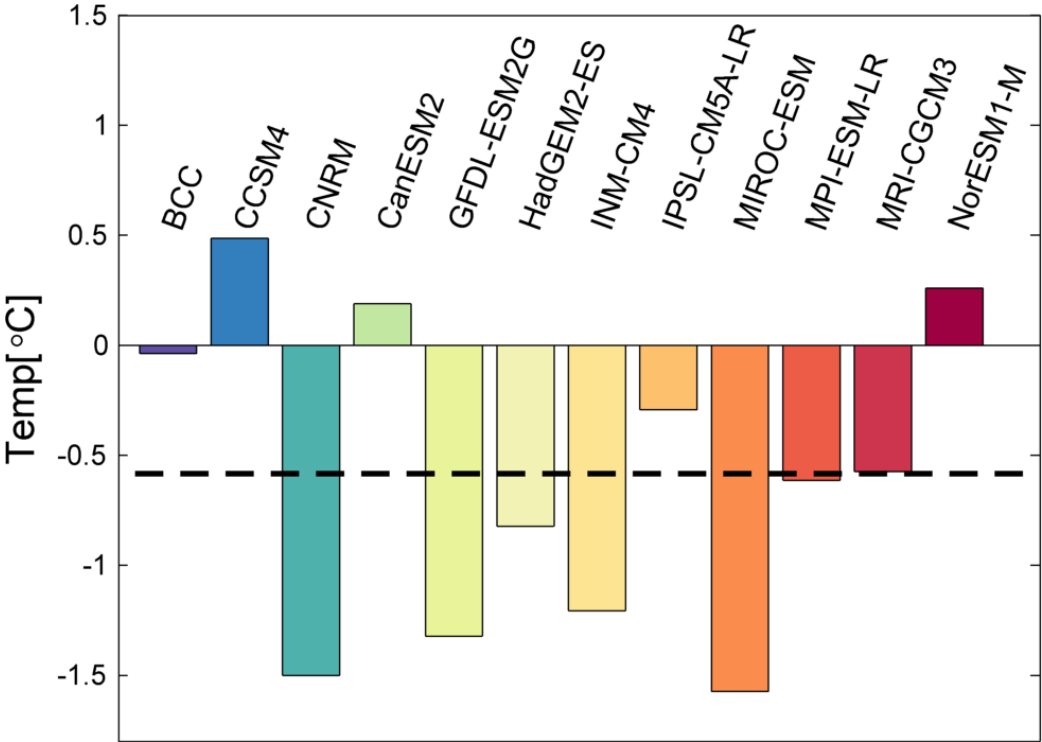


Figure 5: Combined SLR for RCP4.5 (a) and RCP8.5 (b) scenarios. Red and blue line correspond to combined minimum and combined maximum projection. Dashed blue lines approximate timing of ice-shelf collapse. Error bars are displayed where available.

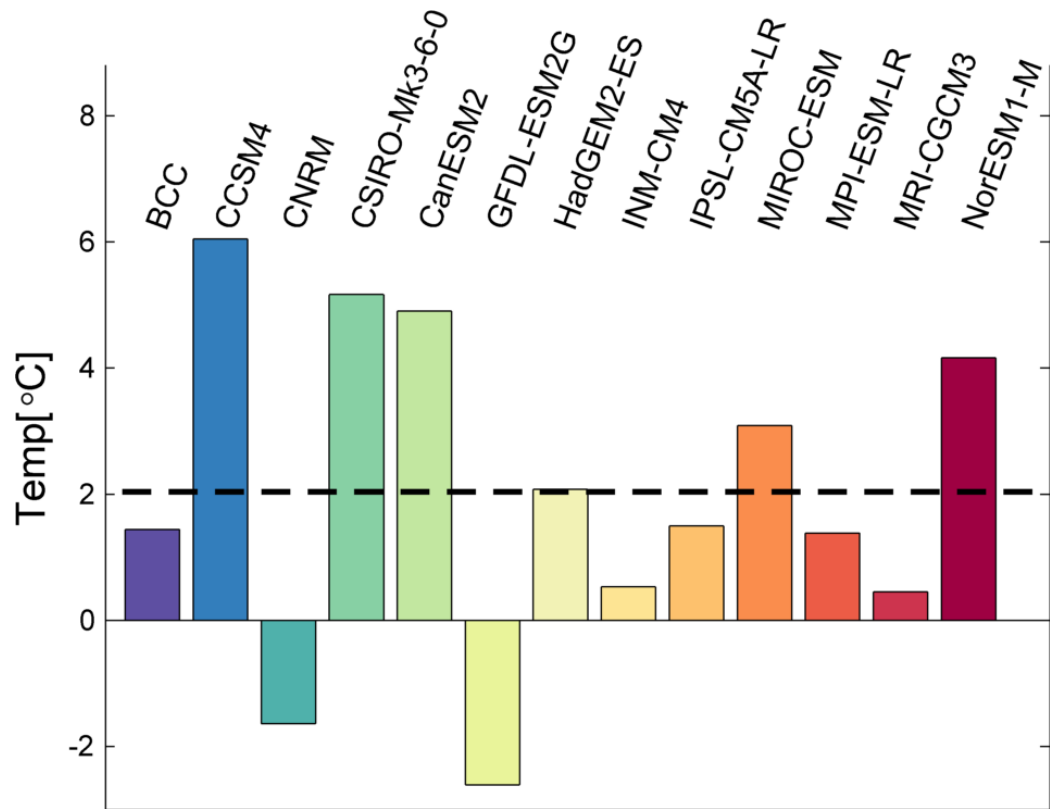
725 **Appendix A. Ocean temperature bias**



726

Figure A.6: Ocean temperature bias in comparison to ERSST v4 from 1979-2005 for each
 727 GCM. Dashed black line indicates multi model mean ($-0.6 \pm 0.7^\circ\text{C}$).

728 **Appendix B. GCM temperature bias**



729

Figure B.7: Near-surface temperature bias in comparison to ERA Interim from 1979-2005.

730 Dashed black line indicates multi model mean ($2.0 \pm 2.6^\circ\text{C}$).

731

Station	Type	Lat	Lon	Height (m.a.s.l)
Bellinghausen	Surface	-62.2	-58.9	16
Biscoe Island	AWS	-66.0	-66.1	20
Bonaparte Point	AWS	-64.8	-64.1	8
Cape Adams	AWS	-75.0	-62.5	25
Deception	Surface	-63.0	-60.7	8
Dismal Island	AWS	-68.1	-68.8	10
Dolleman Island	AWS	-70.6	-60.9	396
Fossil Bluff	AWS	-71.3	-68.3	66
Jubany	Surface	-62.2	-58.6	4
Kirkwood Island	AWS	-68.3	-69.0	30
Limbert	AWS	-75.9	-59.2	58
Marambio	Surface	-64.8	-64.1	198
Marsh	Surface	-62.2	-59.0	10
Racer Rock	AWS	-64.1	-61.6	17
Sky Blue	AWS	-74.8	-71.5	1556
Uranus Glacier	AWS	-71.4	-68.8	753

Table B.2: List of weather stations used to compute the statistical lapse rate. AWS =
732 Automatic Weather Station.